5th SASTech
Iran |Mashhad
May 12 - 17 | 2011
5th Symposium on Advances in Science & Technology

The Effect of the Thickness of Nanoporous TiO_2 Film on the Performance of Nanocrystalline Dye-Sensitized Solar Cell

Masood Hamadanian[1, 2], Afshar Gravand[1], Mostafa Farangi[1], Vahid Jabbari[1*]

[1] Institute of Nanoscience and Nanotechnology, University of Kashan, Kashan, I. R. IRAN

[2] Department of Physical Chemistry, Faculty of Chemistry, University of Kashan, Kashan, I. R. IRAN

Paper Reference Number: 0113-793

Name of the Presenter: Vahid Jabbari

Abstract

Dye-sensitized solar cell (DSSc) consists of a TiO_2 nanostructured film of the photo-electrode, dye molecules on the surface of the TiO_2 film, an electrolyte layer and a counter electrode. Among these, the nanoporous TiO_2 film plays an important role as the photo electrode in DSC because it adsorbs a large number of the dye molecules which provide electrons. Therefore, the condition of the TiO_2 film affects the cell performance such as current density (J_{sc}), open circuit voltage (V_{oc}) and fill factor (FF). The thickness of TiO_2 film is one of these conditions. Its variation influences on the internal impedances of DSC related to the electron transport. As a result, it was observed that the variation of the TiO_2 thickness has an effect on the electron transport in the DSC. The results showed higher efficiency of DSSC for home-made TiO_2 (H-TiO_2) cells with same dependence of cell efficiency on the film thickness for both H-TiO_2 and P25 cells. The best efficiency obtained in this work is 1.82% from H-TiO_2 cell with TiO_2 film thickness of 13µm. The correlation between the TiO_2 films thickness and photoelectron chemical properties of DSSCs fabricated from P25 and H-TiO_2 was compared and discussed.

Keywords: nanoporous titania; electrochemical impedance; N719; Dye-sensitized solar cells

* Corresponding author. Tel: +98 361 5912382; fax: +98 361 5552930
Email: jabbari@grad.kashanu.ac.ir & vahid_jabbari.azeri@yahoo.com

1. Introduction

Photovoltaic technology has been investigated widely as fossil fuel becomes depleted. Especially, a dye-sensitized solar cell (DSC) invented by Michael Grä tzel in 1991 is in the limelight as a promising alternative to the silicon solar cell because of low cost, simple fabrication, flexibility and transparency [O'Regan and Grä tzel (1991); Grä tzel, (2005)]. The operation of the DSC is based on the injection of an electron from photoexcited state of the sensitized dye into the conduction band of the nanocrystalline TiO_2. The electron is transferred to the external load through the nanporous TiO_2 layer. And the sensitized dye is regenerated by the redox system of the electrolyte regenerated itself at the platinum layer of the counter electrode [McFarland and Tang, (2001); Grä tzel, (2001); Park et al., (2000)]. The performance and efficiency of the DSC depend on the platinum layer of the counter electrode, the morphology and the structure of the TiO_2 layer of the photo electrode, dye molecules, the status of the electrolyte and so on. Among these, the thickness of the TiO_2 is an important parameter which affects the performance of the DSC, because this is concerned about the electron diffusion and transport. Therefore, it is necessary to analyze the electron transport on the different thicknesses of the TiO_2 to improve the efficiency of the DSC [Rosidian et al., (1998); Kovtyukhova et al., (1999)]. Many studies on the effect of the TiO_2 thickness, however, have been focused on the transition of open circuit voltage (Voc), current density (Jsc), and fill factor (FF) and the analysis of the incident photon-to-current conversion efficiency (IPCE) [Kang et al., (2004); Kao et al., (2009)]. These are not sufficient to understand the electron transport and diffusion with the different thicknesses of TiO_2 in detail.

Electrochemical impedance spectroscopy (EIS) is an experimental method of analyzing electrochemical systems. This method can be used to measure the internal impedances of the electrochemical system over a range of frequencies. Therefore, this technique is helpful to understand the electrochemical mechanism, the internal resistance and the electron transport of the DSC in varying the thickness of the TiO_2 [Wang et al. (2005)].

This study investigating on the relationship between the thickness of the TiO_2 (P25 and H-TiO_2) and the parameters concerned with the performance of the DSC such as Voc, Jsc, FF and the efficiency was analyzed by using EIS from the viewpoint of the electrochemistry. The changes of the internal resistances with the different TiO_2 thicknesses were analyzed on the basis of the equivalent circuit model for the DSC and the electron life time was analyzed by using the peak frequency from the EIS data to understand the electron transport in varying the thickness of the TiO_2 clearly. Finally, the thickness of the TiO_2 was optimized for the best performance of DSC.

2. Experimental

2.1. Materials and Chemicals

commercially-available TiO_2 powder of P25 (av. 30 nm by Brunauer-Emmett-Teller (BET), 80% anatase (d=21 nm) and 20% rutile (d=50 nm), Degussa, Germany), Titanium (IV) isopropoxide (Merck), acetic acid (Merck), 4-tert-butylpyridine (4-tBP) (Aldrich), acetonitrile (Fluka), valeronitrile (Fluka), hexachloro platinic acid (H_2PtCl_6) (Fluka), Iodine (99.99%, Superpur1, Merck), lithium iodide (LiI) (Merck), ethyl celluloses (30–50 mPas at 5% in toluene:ethanol/80:20 at 258C, #46 080, Fluka), terpineol (anhydrous, #86480, Fluka) and Ru complex dye [Dyesol, cis-bis(isothiocyanato)bis(2,20-bipyridyl-4,40-dicar-boxylato)-ruthenium(II)bis-tetra butyl ammonium: (N719)] were used as received. H2O was purified by distillation and filtration (Milli-Q). $TiCl_4$ (Fluka) was diluted with water to 2M at 0^0C to make a stock solution, which was kept in a freezer and freshly diluted to 40mm with water for each treatment of the fluorine-doped tinoxide (FTO) glass (with a sheet resistance of 15ohm/sq and an optical transmittance of 80% in the visible region) (TEC-15, Dyesol) coated glass plates and surfaces of TiO_2 porous electrodes.

2.2. Preparation of TiO_2 paste. The typical synthesis procedure of H-TiO_2 nanoparticles was adopted from reference [Hamadanian et al., (2009)] with some variations. For preparation of tiatania paste, 15 g of ethyl cellulose (EC) of 10 wt.% ethanolic mixtures were added to a round bottomed rotavap flask containing 3 g TiO_2

and 10 g of terpineol (anhydrous, #86480, Fluka) and diluted with 80 ml of ethanol. This mixture was then sonicated using an ultrasonic horn (Sonics & Materials, Inc), alternating stirring, with a hand mixer (Ultraturrax, IKA), and sonication, for three consecutive times. Ethanol and water were removed from these TiO_2/ethyl cellulose solutions by rotary-evaporator (initial temperature 40 °C). The final screen-printing pastes correspond to 18 wt.% $Ti0_2$, 9 wt.% ethyl cellulose and 73 wt.% terpineol.

2.3. DSSC assembly. The dye-covered TiO_2 electrode and Pt-counter electrode were assembled into a sandwich type cell and sealed with a hot-melt gasket of 25μm thickness made of the ionomer Surlyn 1702 (Dupont). The FTO glass (2cm*2 cm) was firstly treated with an aqueous solution of $TiCl_4$ at 70 ^{0}C for 30 min in order to make a thin compact TiO_2 layer assuring a good mechanical contact between the following coated TiO_2 layer and the FTO substrate. In the second step a transparent layer consisting of TiO_2 particles was doctor blade on the $TiCl_4$-treated FTO. Furthermore, the layers were gradually heated to 500 ^{0}C in order to achieve nanostructured porosity of the TiO_2 layer with a high surface area.
To adsorb a photo sensitized dye on the TiO_2 surface, the TiO_2 working electrode was immersed in a solution of dye in ethanol containing 0.3mM solution of N719 for 24 h at room temperature, immediately after reheating the layers at 100 ^{0}C for 10 min and then rinsed with ethanol. The H_2PtCl_4-treated electrode was prepared by spreading 5 mM H_2PtCl_6 in ethanol on the FTO glass and then heating at 400 ^{0}C for 15 min in air. The PtCl4 treated electrode was placed over the dye-coated electrode and the edges of the cell were sealed with 0.5mm wide strips of 60 mm thick Surlyn (Solaronix, SX1170 Hot Melt). After sealing, an iodide based low viscosity electrolyte with 0.1M LiI, 0.015M I_2, 0.5M 4-tBP in the 5 ml of acetonitrile:valeronitrile (85:15) was injected into the cell. The holes were then covered with small cover glasses and sealed. The irradiated area of the cell was 0.25 cm^2 [Huang et al., (1997)].

2.4. Optical and electrical measurements. The XRD patterns were recorded on a Philips X'pert Pro MPD model X-ray diffractometer using Cu Kα radiation as the X-ray source. The diffractograms were recorded in the 2θ range of 10- 80º. The average crystallite size of anatase phase was determined according to the Scherrer equation. The morphology and size of nanopowders and films were characterized using scanning electron microscope (SEM) (Philips XL- 30ESM) and transmission electron microscope (TEM) (Philips EM208). The absorption spectra of dye solutions and dyes adsorbed on TiO_2 surface were recorded using a UV–vis spectrophotometer (Shimadzu, model UV-3101). EIS spectra are measured with the electrochemical analyzer (Biologic science instrument, SP-150) in the range of the frequency from 100 mHz to 200 kHz.
Photovoltaic measurements employed an AM 1.5 solar simulator. The power of the simulated light was calibrated to be 100 mWcm-2 by using a reference Si photodiode equipped with an IR-cutoff filter (KG-3, Schott), which was calibrated at three solar-energy institutes (ISE (Germany), NREL (USA), SRI (Switzerland)). I-V curves were obtained by applying an external bias to the cell and measuring the generated photocurrent with a Keithley model 2400 digital source meter. The voltage step and delay time of photocurrent were 10MV and 40 ms, respectively. Based on I–V curve, the fill factor (FF) is defined as

$$FF = P_{max} / (J_{sc} \times V_{oc}) = J_{max} \times V_{max} / (J_{sc} \times V_{oc}) \qquad (1)$$

Where J_{max} and V_{max} are the photocurrent and photovoltage for maximum power output (P_{max}), J_{sc} and V_{oc} are the short-circuit photocurrent and open-circuit photovoltage, respectively. The overall energy conversion efficiency (η) is defined as

$$\eta = Jsc \times Voc \times FF / P_{in} \qquad (2)$$

3. Results and discussion

3.1. Optical properties

The UV-vis absorption spectra of the N719 dye and dye sensitized H-TiO_2 electrodes in diluted ethanol solution (10^{-5} mol L^{-1}) are shown in Figure 1. The two broad visible bands at 538 and 398 nm in N719 are assigned to metal-to-ligand charge-transfer (MLCT) origin. The bands in the UV at 314 nm with a shoulder at 304 nm are assigned as intra ligand (π-π^*) charge-transfer transitions [Ito (2005)]. When the dye is adsorbed on TiO_2 surface, the absorption Spectra of this dye is broadened and blue-shifted more or less as compared to that in solutions, The similar phenomenon was also observed for other organic dyes [Menzies et al., (2003)]. The trend may ascribe to H-type aggregation of the dye on the TiO_2 surface. It is also obvious from the figure that there is higher absorbance in the ultraviolet region due to its absorption by the TiO_2 nanoparticles rather than the dye molecules whereas the absorption in the visible region is attributed to the absorption by dye molecules.

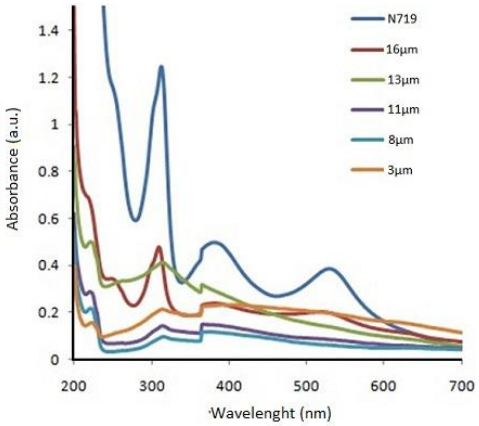

Figure 1. Light absorption spectra of dye solutions of N719 and TiO2-H in different thickness of 3 µm to 17µm.

3.2. Spectroscopy analysis

3.2.1. nanoparticles

Figure 2 shows the X-ray diffraction patterns of the P25 and H-TiO_2. The nanocrystalline anatase structure was confirmed by (101), (004), (200), (105) and (211) diffraction peaks [Ogawa and Abe, (1981)]. Typical peaks in XRD pattern are observed at 2θ values 25.28 º, 38.08 º and 47.92 º, which assigned to 10 1, 004 and 200 planes, respectively, while the main peaks of rutile and brookite phases are at 2θ = 27.4º (110 plane) and 2θ = 30.8º (121 plane). For P25, the major phase is anatase (25.2, 37.7, 48.0, 54.0, and 54.9°, JCPDS 21–1272), with the minor rutile phase (27.3, 36.0, 41.2, 44.0, 54.3, and 56.6°, JCPDS 21–1276). The average crystal size was estimated from the Scherer equation on the anatase (2θ =25.2º) diffraction peaks (the most intense peaks for each sample were calculated to be around 20-30 and 15-20nm for P25 and H-TiO_2, respectively.

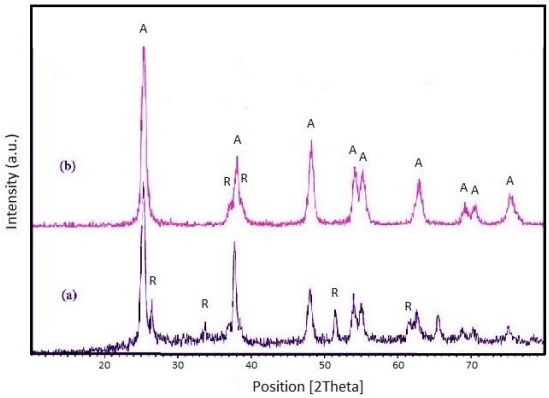

Figure 2. XRD patterns of P25 (a) and H-TiO_2 (b) nanoparticles.

SEM micrograph of the calcined (500 ºC) H-TiO_2 nanoparticles is shown in Figure 3. This image shows global and uniform particles. Further observation indicates that the morphology of samples is very rough and may be beneficial to enhancing the adsorption of dye due to its great surface roughness and high surface area. Figure 3 also shows the TEM image of H-TiO_2 nanoparticles. It can be seen that the sample consist of well-dispersed nanoparticles whose particle size of TiO_2 was found to be around 15-20nm.

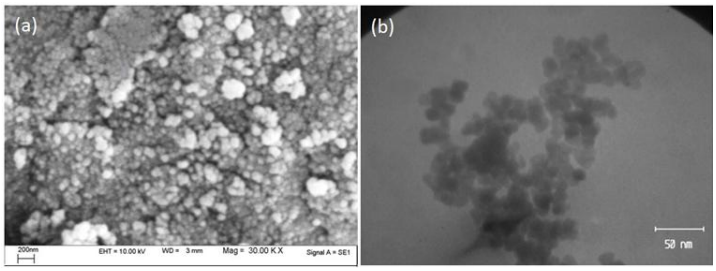

Figure 3. SEM (a) and TEM (b) images of H-TiO_2.

3.2.2. Film electrodes

The SEM micrograph of TiO_2 film made of H-TiO_2 sample (Figure 4(a)) shows a rough surface layer containing large TiO_2 chunks in which the individual TiO_2 particles are hardly visible. The chunk structure is likely formed through the aggregation of TiO_2 arranged in a side-by-side configuration. Another possible reason for the appearance of irregular chunks on the TiO_2-H layer is the stress-induced surface rumpling caused by the fast cooling after 500 ^{0}C calcination. It can be seen clearly that nanoparticle clusters and lots of nanopores existed in the film, while the nanoporous morphology and interconnectivity among the TiO_2 particles with lots of unequal pores distributed in the films can be observed. Also, it can be seen that the film is composed of micro-scale and sub-micro-scale near spherical clusters containing TiO_2 nanoparticles, while the size of TiO_2 nano-particles is about 20 nm. This kind of thin film materials with hierarchical structure containing micro, sub-micro- and nano-scale elements may be of benefit for the achievement of various photo-electric properties.

The chunk-free and almost smooth area exhibits more compact structure than the P25 based film as shown in Figure 4(b). Presumably, this is due to the small TiO_2 particles forming the high density film. It is also noted from Figure 4(b) that the film made from P25, even with high porosity, showed appearance of breaks which may influence the electron transport and result in lower cell efficiency than that of H-TiO_2 (see the next section). The H-TiO_2 nanoparticles, on the other hand, can restrict the constriction resulting in the continuous less-crack and porous films upon calcination. Nevertheless, for both TiO_2 films, the crack produced voids in the preceding layer can be filled by the H-TiO_2 and P25 paste during the next doctor blade process.

Also, Figure 4(c,d) shows the SEM micrograph of a cross-section of the H-TiO_2 photo electrode which reveals the thickness of the fabricated electrode with one time doctor blade, where TiO_2 film with thickness 3μm (for one-time doctor blade) and 13μm (for five-time doctor blade) lies on the top of FTO film. The image also shows that the electrode has nearly uniform thickness which is an important criterion to obtain good cells with high efficiency.

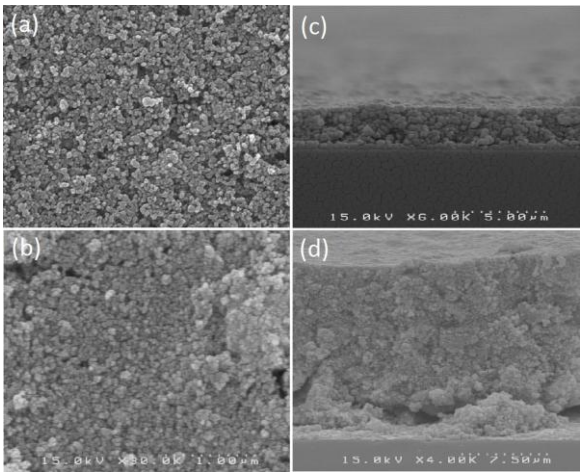

Figure 4. SEM images of the surface of P25 film (a), H-TiO2 film (b), cross-section of the H-TiO2 film fabricated with one-time (c) and five-time doctor blade (d).

3.3. Evaluation of DSC performance

The above prepared H-TiO_2 and P25 photoelectrodes were used to fabricate the solar cells for photoelectrochemical performance study [Fujishima and Honda, (1972); Grä tzel, (2001)]. Figure 5(a) showed the typical current-voltage characteristics of N719-sensitized DSSCs for various film thickness of H-TiO_2 films. Table 1 lists the photoelectric data of the DSSCs including the amount of dye adsorbed on TiO_2 (A_{dye}), the short-circuit photocurrent density (J_{sc}), the open circuit voltage (V_{OC}), the fill factor (FF), and the conversion efficiency (η). It is apparent that the DSSC performance largely depends on the TiO_2 film thickness because changing the film thickness changes A_{dye}, J_{sc}, and, η owing to the change of total TiO_2 surface area [Guo et al., (2008); Kao et al., (2009)]. It is found that there is a parallel increase of efficiency for H-TiO_2 cells and P25 cells for TiO_2 film thickness up to 13μm and 15μm, respectively. Further increase in the thickness stabilizes the efficiency at an almost decreased value upon increasing the thickness of TiO_2 thin films. The maximum efficiency acquired in DSSC using the H-TiO_2 with film thickness of 13μm was 1.82% with J_{sc} of 4.9 mA/cm2, V_{oc} of 0.69 V, and FF of 0.54; while η of the cell using P25 with film thickness of 14μm reached 1.4% with Jsc of 3.8 mA/cm2, V_{oc} of 0.67V, and FF of 0.55. It is generally believed that thicker TiO2 film would uptake more N719 molecules leading to the enhancement in the photocurrent of the DSSC. Therefore, the thickness of the TiO_2 is a dominant parameter which influences on the performance of the DSC [Han et al., (2004); Wu et al., (2007)]. This result indicates the limited electron transport for thick films due to the increase of recombination centers and requisite path length of the injected electron to be collected by FTO. Moreover, when the TiO_2 films are thicker, the films become less transparent which is detrimental to the light harvesting as well as DSSC performance. Based on Table 1, the H-TiO_2 cells in general have superior performance than P25 cells. The efficiency and current density from average of seven H-TiO_2 cells present in Table 1 are about 30% (η) and 29% (Jsc) higher than those from average of seven P25 cells. Higher efficiency and current density might be attributed to, first, the higher amount of adsorbed N719 for the each cell, owing to larger surface area (because of lower nanoparticle size) of powder and more compact structure of H-TiO_2 film. Higher UV absorption intensity of the N719 adsorbed on H-TiO_2 film than P25 film (not shown) also supports this conclusion. Secondly, it could be due to the less cracks of H-TiO_2 films (see Figure 4) which improved the short-circuit photocurrent [GoHmez et al., (1999)].

Cell type	Thickness (μm)	A_{dye}[a] (mmol/cm^2)	J_{sc} (mA cm−2)[b]	V_{oc} (mV)[c]	FF (%)[d]	η (%)[e]	τ (s)
H-TiO2	3	0.16	1.68	0.69	0.52	0.6	0.007
H-TiO2	5	0.53	2.1	0.59	0.58	0.72	0.0084
H-TiO2	8	1.2	2.9	0.61	0.5	0.89	0.01
H-TiO2	11	1.37	3.3	0.62	0.55	1.1	0.011
H-TiO2	13	1.74	4.9	0.69	0.54	1.82	0.016
H-TiO2	15	1.89	4.1	0.69	0.52	1.47	0.016
P25	4	0. 11	1.3	0.65	0.57	0.48	0.005
P25	6	0. 32	1.78	0.66	0.56	0.66	0.0104
P25	9	0. 68	2.64	0.65	0.58	0.99	0.0133
P25	11	0.96	3.2	0.64	0.57	1.17	0.0155
P25	14	1.15	3.8	0.67	0.55	1.4	0.017
P25	16	1.33	3.5	0.64	0.56	1.25	0.016

[a] A_{dye}: amount of dye adsorbed on TiO2.
[b] J_{sc} is the short circuit current density.
[c] V_{oc} is the open circuit voltage.
[d] FF is the fill factor.
[e] η is the overall conversion efficiency.

Table 1. The performances and the electron lifetime(s) of the DSC fabricated by H-TiO2 and P25 electrodes with the different film thicknesses.

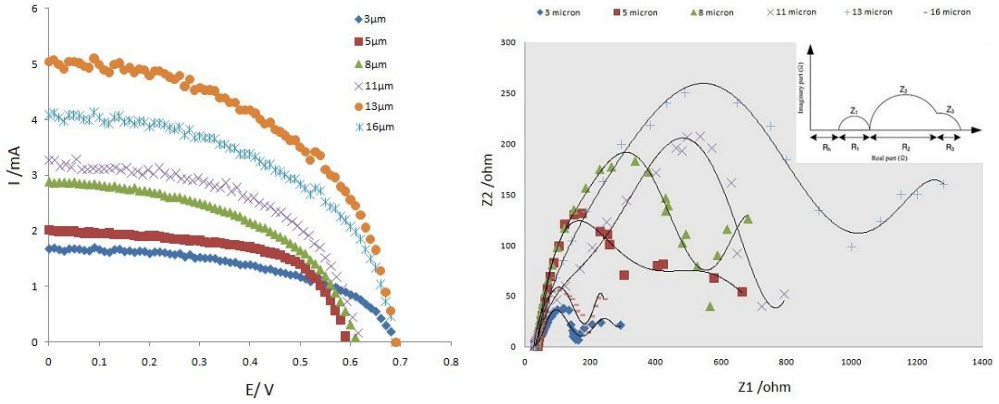

(a) **(b)**

Figure 5. Photocurrent-voltage characteristics (a) and EIS spectra (b) of DSSCs fabricated of H-TiO2 with different thicknesses of films.

For electron transport analysis of effect of film thickness on the cell efficiency, EIS was applied. There are four internal impedances in the DSC on the basis of the equivalent circuit model. These impedances have a great effect on the electron transport in the mechanism of the DSC. Figure 5(b) shows a typical Nyquist diagram of a DSC from the result of EIS analysis. It is shown that four internal impedances are the impedance (Z_3) related to the Nernstian diffusion within the electrolyte in the low-frequency peak (in the mHz range), the impedance (Z_2) related to the electron transport in the TiO_2/dye/electrolyte interface in the middle-frequency peak (in the 1–100

Hz), the impedance (Z_1) related to the charge transfer at the platinum counter electrode in the high-frequency peak (in the kHz range) and the sheet resistance (R_h) of the FTO in the high frequency range over 1 MHz) [Koide et al., (2006); Han et al., (2004)]. These impedances consist of the resistances of the real part axis and the capacitances of the imaginary part axis. The capacitance components are abbreviated because the DSC is operated in the DC conditions. Therefore, total internal impedances of the DSC are expressed the sum of the resistance components (R_1, R_2, R_3, and R_h). And the performance of the DSC becomes high when this total internal resistance is small.
Figure 5(b) shows the EIS spectra of H-TiO_2 based electrodes with different thickness. As shown in Figure 5(b), the second semi-circle is reduced as the TiO_2 thickness is increased up to 13μm. In other words, the resistance related to the electron transport in the TiO_2/dye/electrolyte interface (R_2) is decreased. This induces the reduction of the total internal resistance and the improvement of the efficiency. This means that the electron diffusion and transport become easy with the increment of the TiO_2 thickness, because the number of dye molecules is increased. As shown in Figure 1 (previous section), the light absorption increases in the region from 400 nm to 600 nm as the thickness of the TiO_2 increases. This explains that more dye molecules are attached to the increased surface of TiO2. Then, it can generate many electrons and improve the electron transport.
The electron diffusion length becomes longer as the electron lifetime increases. The electron lifetime (τ) is calculated by Eq. (3) using the peak frequency (f) of the second semi-circle from the Nyquist diagram [Hoshikawa et al., (2006)]; $\tau = 1/\pi f$. Electron lifetime of H-TiO_2 and P25 based electrodes with the different thicknesses are shown in Table 1. The peak frequency decreases and the electron lifetime increases as the thickness of TiO_2 increases. The increase of the electron lifetime makes the electron diffuse and transfer more easily due to the increase of the diffusion length. The current density and the efficiency are increased as the H-TiO_2 and P25 thickness increases up to 13 and 14μm, respectively, because the internal resistance related to the electron transport in the TiO_2/dye/electrolyte interface is decreased and the electron lifetime is increased. The performance of the DSC with the higher thickness, however, is decreased because the recombination of the electron is strengthened. Finally, it is demonstrated that the optimal TiO_2 thickness is 13μm (for H-TiO_2) and 14μm (for P25) for the best performance of the DSC.

4. Conclusions

The thickness of TiO_2 film of the photo-electrode is a significant parameter which affects the performance of the DSC. The increase of the TiO_2 thickness is accompanied by the decrease of the internal resistance related to the electron transport in the TiO_2/dye/electrolyte interface and the increase of the electron lifetime. This causes the improvement of the electron diffusion and transport in the TiO_2 layer, which causes the improvement of the efficiency. The excessive thickness of the TiO_2, however, is not good for the performance of the DSC because of the electron recombination. It is analyzed by the Nyquist diagram from the EIS result based on the equivalent circuit model of the DSC. Finally, the TiO_2 thickness for the best performance of the DSC is optimized with the thickness of 13μm. The H-TiO_2 film shows more compact structure with consistent and superior DSSC performance than P25 based cells. This could be due to the higher amount of adsorbed N719 on H-TiO_2 film, less cracks of H-TiO_2 film, and faster electron transport of H-TiO_2 film

Acknowledgment. The authors gratefully acknowledged the financial support of Iran government grant for the financial support of this work which made the study possible.

References

(1) McFarland, E.W., Tang, J. (2010). Nature, 421, 616–618.
(2) Fujishima, A., Honda, K. (1972). Nature, 238,5358, 37–38.
(3) Gratzel, M. (2001). Nature, 414, 338–344.
(4) GoHmez, M., RodrmHguez, J., Tingry, S., Hagfeldt, A., Lindquist, S.-E., Granqvist, C.G. (1999). Solar Energy Materials & Solar Cells, 59, 277-287.

(5) Gratzel, M. (2005). Inorg. Chem, 44, 6841–6851.
(6) Guo, Y., Lee, N.-H., Oh, H.-J. (2008). Thin Solid Films, 516 ,23, 8363–8371.
(7) Hamadanian, M., Reisi-Vanani. A., Majedi. A. (2009). Materials Chemistry and Physics,116, 376–382.
(8) Han, L., Koide, N., Chiba, Y., Mitate, T. (2004). Applied Physics Letters, 84 (13), 2433–2435.
(9) Hoshikawa, T., Ikebe, T., Kikuchi, R. (2006). Eguchi K. Electrochim. Acta, 51, 5286–5294.
(10) Huang, S Y., Schlichthorl, G., Nozik, A J., Grä tzel, M., Frank, A. J. (1997). J. Phys. Chem. B, 101, 2576.
(11) Ito, S. (2005). Chem. Commun, 4351.
(12) Kang, M.G., Ryu, K.S., Chang, S.H., Park, N.G., Hong, J.S., Kim, K.J. (2004). Bull. Korean Chem. Soc, 25, 742–744.
(13) Kao, M.C., Chen, H.Z., Young, S.L., Kung, C.Y., Lin, C.C. (2009). Thin Solid Films, 517, 5096–5099
(14) Koide, N., Islam, A., Chiba, Y., Han, L. (2006). J. Photochem. Photobiol. A Chem, 182, 296–305.
(15) Kovtyukhova, N., Ollivier, P. J., Chizhik, S., Dubravin, A., Buzaneva, E., Gorchinskiy, A., Marchenko, A., Smirnova, N. (1999). Thin Solid Films, 337. 166.
(16) Menzies, D., Cervini, R., Cheng, Y-B., Simon, G., Spiccia, L. (2003). J. Aust. Ceram. Soc, 39 (108).
(17) Ogawa, H., Abe, A. (1981). J. Electrochem. Soc, 128, 685.
(18) O'Regan, B., Grä tzel, M. (1991). Nature, 353, 737–740.
(19) Park, N.G., van de Lagemaat, J., Frank, A.J. (2000). J. Phys. Chem, 104, 8989–8994.
(20) Rosidian, A., Liu, Y. J., Claus, R. (1998). Adv. Mater, 10, 1087.
(21) Wang, Q., Moser, J.E., Grätzel, M. (2005). J. Phys. Chem. B, 109, 14945–14953.
(22) Wu, J.-J., Chen, G.-R., Yang, H.-H., Ku, C.-H., Lai, J.-Y. (2007). Applied Physics Letters, 90 (21).